Neuroscience 361 (2017) 157–166

EXCITATORY EFFECTS OF THE PRIMARY AUDITORY CORTEX ON THE SOUND-EVOKED RESPONSES IN THE IPSILATERAL ANTERIOR AUDITORY FIELD IN RAT

GUANGWEI ZHANG,[a] CAN TAO,[a,b] CHANG ZHOU,[a] SUMEI YAN,[a] ZHAOQUN WANG,[a] YI ZHOU[a]* AND YING XIONG[a]*

[a] *Department of Neurobiology, Chongqing Key Laboratory of Neurobiology, Third Military Medical University, 30 Gaotanyan St., Chongqing 400038, China*

[b] *208 Hospital, 4799 Xi'an Rd, Changchun 130062, China*

Abstract—In the neocortex, interaction and cooperation between different areas are important for information processing, which also applies to different areas within one sensory modality. In the temporal cortex of rodents and cats, both the primary auditory cortex (A1) and the anterior auditory field (AAF) have tonotopicity but with a mirrored frequency gradient. However, whether and how A1 modulates the responses in AAF is largely unknown. Here, we functionally identified the locations of A1 and AAF in rats and used an optogenetic approach to manipulate the activity of A1 in vivo. We found that activation of A1 axon terminals in AAF did not change AAF responses, but activating A1 neuronal cell bodies could increase the sound-evoked responses in AAF, as well as decrease the intensity threshold and broaden the frequency bandwidth, while suppressing A1 could cause the opposite effects. Our results suggested that A1 could modulate the general excitability of AAF through indirect pathways, which provides a potential relationship between these two parallel auditory ascending pathways.

Key words: multiunit recording, parallel auditory pathway, interaction, terminal activation.

INTRODUCTION

The auditory cortex consists of several areas, which are identified according to their specific response properties (e.g., tonotopicity and monotonicity) and the anatomical connections of each area in rat (Doron et al., 2002; Rutkowski et al., 2003; Polley et al., 2007; Shiramatsu et al., 2016; Tao et al., 2017) and mice (Guo et al., 2012; Issa et al., 2014; Joachimsthaler et al., 2014). Among these regions, the primary auditory cortex (A1) and anterior auditory field (AAF) are both tonotopically organized, in rat (Doron et al., 2002; Polley et al., 2007; Tao et al., 2017), cat (Imaizumi et al., 2004) and mouse (Hackett et al., 2011; Issa et al., 2014). Previous studies have revealed that A1 and AAF are both reciprocally connected with the medial geniculate body (MGB) in rat (Winer et al., 1999) and cat (Andersen et al., 1980; Rouiller et al., 1991; Lee et al., 2004), but how A1 affects the responses in AAF is largely unknown. Previous studies found that AAF receives monosynaptic projections from auditory thalamus (Andersen et al., 1980; Morel and Imig, 1987; Lee et al., 2004) and A1 (Lee and Winer, 2008) in cat, thus A1 could potentially modulate AAF via direct (e.g. cortico-cortical connections) or indirect (e.g. cortico-thalamic loop) pathways.

Extensive studies have found corticocortical interactions between different areas in other modalities, including visual cortex (Girard and Bullier, 1989; Girard et al., 1991) and somatosensory cortex (Pons et al., 1987; Turman et al., 1995). However, little is known about the functional relationship between A1 and AAF. In cats, AAF deactivation using reversible cooling can suppress tone-evoked responses in ipsilateral A1 (Carrasco and Lomber, 2009), and auditory cortex (including A1 and AAF) deactivation can modulate responses of contralateral AAF (Carrasco et al., 2015). Still, there is little clear evidence regarding how A1 affects the neuronal responses in the ipsilateral AAF.

To examine whether and how A1 modulates the activity of ipsilateral AAF, we used anterograde and retrograde tracing, confirming the direct corticocortical projections from A1 to ipsilateral AAF. Then we applied an optogenetic approach to specifically manipulate the A1 axon terminals in AAF, but we failed to observe statistically significant changes in tone-evoked responses, which suggest that A1 cannot modulate tone-evoked responses via direct A1–AAF projections. However, we found that activating cell bodies in A1 enhanced the sound-evoked responses, decreased intensity threshold and broadened frequency bandwidth in AAF, while A1 deactivation resulted in opposite effects. Together, our results suggest that A1 indirectly modulates the general excitability of AAF, which is a

*Corresponding authors. Address: Department of Neurobiology, Chongqing Key Laboratory of Neurobiology, Third Military Medical University, Chongqing, China.
E-mail addresses: zhouyisjtu@gmail.com (Y. Zhou), xiongying2001@163.com (Y. Xiong).

Abbreviations: A1, primary auditory cortex; AAF, anterior auditory field; AAVs, adeno-associated viruses; CF, characteristic frequency; ChR2, channelrhodopsin; eGFP, enhanced green fluorescent protein; eNpHR, express halorhodopsin; LFP, local field potential; PBS, phosphate-buffered saline; TRF, tonal receptive field.

http://dx.doi.org/10.1016/j.neuroscience.2017.08.019
0306-4522/

salient functional relationship between these two cortical areas.

EXPERIMENTAL PROCEDURES

Animal preparation and surgery

All procedures were approved by the Animal Care and Use Committee of the Third Military Medical University. All experiments were performed according to relevant guidelines. Adult Sprague–Dawley rats (female, 2 months, 180–210 g) were used in this study. Animals were first anesthetized using urethane (1.5 g/kg), with an additional dose given if hind paw retraction was evoked by toe pinch. Body temperature was continuously monitored and maintained at 37 °C using a heating pad with a feedback controller. Animals were head-fixed using a customized apparatus as previously described (Tao et al., 2016). A standard craniotomy procedure was used to expose the right auditory cortex (bregma −2 mm to −7 mm on the temporal skull).

Functional localization of A1 and AAF

After craniotomy, the tungsten electrode (0.1 MΩ, WPI Inc., Sarasota, FL, USA) was inserted to the depth of 450 μm below the pia (Fig. 1A), which corresponds to layer (L) four of the auditory cortex (Ehret and Romand, 1997; Tao et al., 2016). The tonal receptive field (TRF) was obtained for each recording site. Then, the tonotopic map was reconstructed based on the characteristic frequency (CF) of every recording site. According to previous reports, the CF in A1 increases from caudal to rostral, with the reverse pattern in the anterior auditory cortex (Polley et al., 2007; Tao et al., 2017). For systematic mapping of A1 and AAF, at least 10 sampling points for each area were obtained. To determine the center of 1–10 kHz areas in A1 and AAF, a Delaunay triangulation was first performed based on the tonotopic map, and Voronoi diagram was generated based on Delaunay triangulation. Then polygons were merged if their CFs are within the 1–10-kHz ranges. The centroid of the irregular merged polygon is determined as the center of 1–10-kHz areas for A1 and AAF (Fig. 1D).

Sound stimulation

To obtain the TRF, pure tones of various frequency and intensity combinations (0.5–64 kHz, 0.1-octave step; 0–70 dB, 10 dB step, totally 568 pure tones) were pseudo-randomly delivered (interval, 200 ms). The duration of each pure tone was 35 ms, with 5-ms cosine ramp. Then, the TRF of the neuronal population or single cell was reconstructed based on the evoked responses via customized MATLAB software (Mathworks, Inc. Natick, MA, USA). The sound waveform was generated using customized Labview Software (National Instrument, Inc. Austin, TX, USA), and then the signals were amplified via a TDT speaker driver (SA1, TDT Inc., Alachua, FL, USA) and delivered via a free-field magnetic speaker (MF1, TDT Inc. Alachua, FL, USA).

All of the sound stimuli were calibrated. The sound was captured using a 1/4-inch pressure microphone (377A01, Piezotronics Inc., Depew, NY, USA), a pre-polarized condenser (426B03, Piezotronics Inc., Depew, NY, USA) and a signal conditioner (480E09, Piezotronics Inc., Depew, NY, USA). Then, the signal was transferred to a DAQ board (PCI-6251, National Instruments, Austin, TX, USA). All the sound distortions were less than 0.1 dB after calibration. The speaker was placed on the left side of the animal and 5 cm away from the ear canal.

Adeno-associated virus injection

Adult Sprague–Dawley rats were anesthetized with a mixture of ketamine (55 mg/kg) and xylazine (6.4 mg/kg), and a small craniotomy (1 mm^2) was performed in the presumed location of A1 (5–6 mm posterior to bregma) on the temporal skull. Then we obtained TRFs within the craniotomy window and adjusted the craniotomy window to make sure the CF of the injection site was within the 1–10 KHz. Once we located the lower-to-middle frequency region of AAF, the following adeno-associated viruses (AAVs) encoding ChR2 and eNpHR3.0 were used depending on the purpose of the experiments. AAV2/8-CaMKIIa-eGFP (titer, 1×10^{13}, Neuron Biotech Co., Ltd. Shanghai, China) was used to express enhanced green fluorescent protein (eGFP) on excitatory neurons as negative control for optogenetic experiments; to express channelrhodopsin (ChR2) on excitatory neurons, AAV2/5-CaMKIIa-hChR2-mCherry (titer, 1 x 10^{13}, Neuron Biotech Co., Ltd. Shanghai, China) was used; to express halorhodopsin (eNpHR) on excitatory neurons, AAV2/8-CaMKIIa-eNpHR3.0-eYFP (titer, 1×10^{13}, Neuron Biotech Co., Ltd, Shanghai, China) was used. The virus was injected using a broken glass pipette (opening: 20 μm) attached to a microsyringe pump (UMP3, WPI Inc., Sarasota, FL, USA). For each injection, 0.5–1 μl of the virus was injected at a rate of 40 nl min^{-1}. After each injection, the pipette was left at the injection site for 10 min before withdrawal. For animals with the diameter of the craniotomy window larger than 1 mm^2, the window would be covered using Kwik-Cast Sealant (WPI Inc., USA). Then, the scalp was sutured, and the animals were returned to their home cages. The animals were allowed to recover for at least 4 weeks before experiments were performed.

Tracer injection and imaging

For retrograde tracing from AAF to A1, 1 μl of fluorescently conjugated Cholera toxin subunit B (CTb 488, 0.25% in PBS; Invitrogen, Waltham, MA, USA) was injected into AAF using the same method as described above. The animal was allowed to recover for at least 1 week. For anterograde tracing, AAV2/8-CaMKIIa-eGFP (titer, 1×10^{13}, Neuron Biotech Co., Ltd. Shanghai, China) was used to express eGFP on excitatory neurons. The animal was allowed to recover for at least 3 weeks. Then the animals were deeply anesthetized using urethane and transcardially perfused with 4% paraformaldehyde. Next, the rat brain was sliced into 200-μm sections using a vibratome, and then

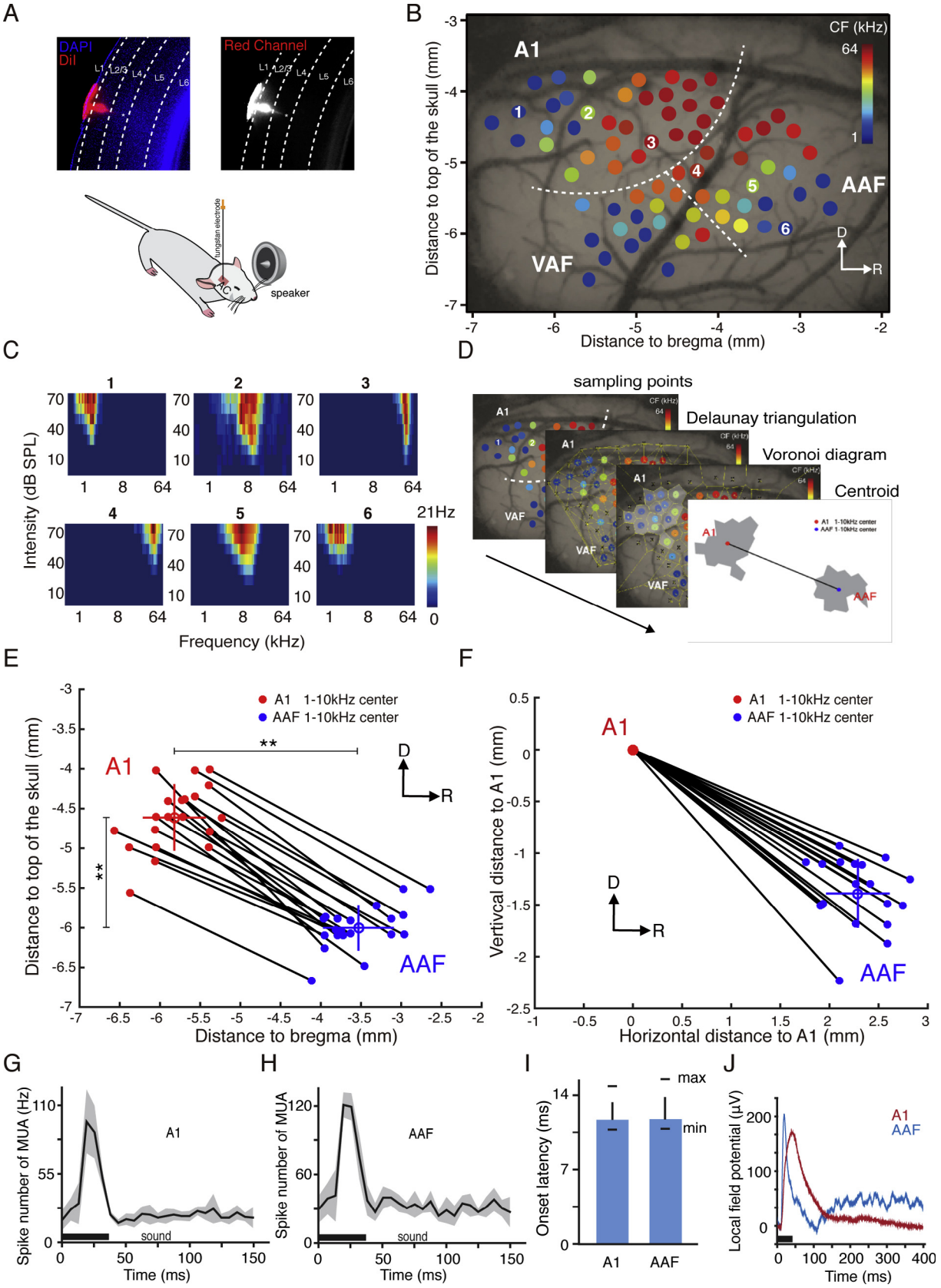
A
DAPI
DiI
L1
L2/3
L4
L5
L6
Red Channel
tungstan electrode
speaker
B
A1
AAF
VAF
CF (kHz)
64
1
D
R
Distance to top of the skull (mm)
Distance to bregma (mm)
C
Intensity (dB SPL)
Frequency (kHz)
21Hz
D
sampling points
Delaunay triangulation
Voronoi diagram
Centroid
E
A1 1-10kHz center
AAF 1-10kHz center
Distance to top of the skull (mm)
Distance to bregma (mm)
F
Vertivcal distance to A1 (mm)
Horizontal distance to A1 (mm)
G
Spike number of MUA (Hz)
Time (ms)
sound
H
I
Onset latency (ms)
max
min
J
Local field potential (μV)
Time (ms)

the brain slices were mounted onto glass slides and imaged using a confocal microscope. The low-frequency center of AAF was 2.3 ± 0.3 mm more anterior (n = 20, p < 0.01, paired t test), and 1.4 ± 0.3 mm more ventral (n = 20, p < 0.01, paired t test) than that of A1, so the brain sections contained AAF could be identified based on the relative distance with the injection site (A1).

Immunohistochemistry

Immunohistochemistry reactions were used to investigate the specificity and efficiency of the expression of AAV. Four weeks after the injection of the virus, the brain was cut into frozen sections (CM1900 cryostat, Leica GmbH, Buffalo Grove, IL, USA) at a thickness of 35 μm. The sections were rinsed 3 times (5 min each) in phosphate-buffered saline (PBS), and then the sections were transferred into Triton X-100 (0.5% in PBS) for 30 min at room temperature. Then, these sections were incubated with bovine serum (2% in PBS) for 1 h, followed by washing three times with PBS. After this, these sections were incubated with a CaMKIIa primary antibody (mouse anti-CaMKIIa, 1:100, C265, Sigma-Aldrich, St. Louis, MO, USA) at 37 °C for 4 h. Then, sections were rinsed 3 times (10 min each) with PBS. After this, these sections were incubated with secondary antibody (goat anti-rabbit conjugated with FITC, 1:100, ZF-0311, ZSGB-BIO, Tianjin, China) at 37 °C for 2 h. Then, the reactions were stopped by transferring the sections into PBS and rinsing twice (3 min each). Next, the sections were mounted onto glass slides, and images were collected using a fluorescent microscope (Olympus, Center Valley, PA, USA).

Laser stimulation

To activate ChR2, an optic fiber (diameter, 250 μm, Thorlabs, Inc., Newton, New Jersey, USA) that coupled with a blue laser (473 nm, Newdoon Inc., Shanghai, China) was placed near the cortical surface. The laser power measured at the end of the optic fiber was 8 mW, and the light stimulation spanned the area of interest. Light-evoked multi-unit responses in A1 were obtained to check the efficiency of A1 activation. To photo-activate eNpHR3.0, a yellow (589 nm, Newdoon Inc., Shanghai, China) laser was used, and the power measured at the end of the optic fiber was 8 mW. The power of the laser was calibrated using a power and energy meter (Thorlabs, Inc., Newton, New Jersey, USA) for each experiment.

In vivo electrophysiological recording

The multi-unit responses were obtained using tungsten electrodes (0.1 MΩ, WPI Inc., Sarasota, FL, USA) at the depth between 450 to 480 μm below the pia. The signal was amplified and collected using the TDT System 3 (sampling rate: 50 kHz, TDT Inc., Alachua, FL, USA). The tungsten electrode was manipulated using a powered micromanipulator (DMA-1511, Narishige, Setagaya-ku, Tokyo, Japan), which could also read the depth of the tip of the electrode. A Bessel band-pass filter was used to separate multi-unit activity (300–3000 Hz) and local field potential (1–300 Hz). We used 3*SD of the baseline (collected within a 50-ms window before sound stimulation) to detect MUA and LFP. Histological reconstruction of electrode tracks was performed after each experiment as we previously described (Tao et al., 2016; Tao et al., 2017). In short, the electrode was coated with 1,1′-Dioctadecyl-3,3,3′,3′-Tetramethylindocarbocyanine Perchlorate (DiI, ThermoFisher, Inc., Waltham, MA, USA) and the brain slices were imaged after experiments.

Data analysis

Online data analysis was performed using Brainware (TDT Inc., Alachua, FL, USA), and the offline analysis was performed using customized MATLAB software (Mathworks Inc., Natick, MA, USA). Statistical analysis was performed using SPSS (IBM Inc., Armonk, New York, USA) and Office Excel (Microsoft Co., Redmond, WA, USA). To compare responses before and after light stimulation, paired t tests were used. The intensity threshold for each recording was determined as the lowest intensity that could evoke responses. The CF was determined as the frequency with the lowest sound level that could evoke responses. Because the averaged onset latency of sound-evoked responses in AAF L4 was 11.4 ms (Fig. 1H), the evoked activity was defined as the averaged spiking rate 10–25 ms after the onset of sound stimulation. Spontaneous activity was defined as the averaged spiking rate measured within a 50-ms window before the onset of sound stimulation. The standard deviation was used unless otherwise specified.

RESULTS

Localization of A1 and AAF

To comprehensively characterize the influence of the A1 on the anterior auditory cortex in rats, we first applied

Fig. 1. Functional localization of the primary auditory cortex and the anterior auditory cortex. (A) Schematic drawing of the recording setup. The animal's head was fixed using a customized apparatus. Upper panel, an example image shows the track of the tungsten electrode, * indicates the position of the electrode tip. (B) An example tonotopic map in the right auditory cortex. Each dot corresponds to one recording site, and the color indicates its characteristic frequency (CF). A1, primary auditory cortex; AAF, anterior auditory field; VAF, ventral auditory field; D, dorsal. (C) Multi-unit tonal receptive fields of recording sites in (A); color represents firing rate. (D) The pipeline used to determine the center of 1–10-kHz areas of A1 and AAF. (E) Positions of low-frequency centers for A1 and AAF; data from the same animal are connected by a line, n = 21, $^{**}p$ < 0.01, paired t test. Error bar, SD. Circle, averaged coordinate. (F) Relative positions of A1 and AAF; positions of low-frequency centers in A1 across different animals have been aligned, n = 21. Error bar, SD. (G–H) Peri-stimulus-time histogram of A1 and AAF; the shaded area represents the standard deviation. (I) Comparison of the onset latency of sound-evoked responses in A1 and AAF. Error bar, SD, n = 35 for A1 and n = 42 for AAF. (J) Sound induce LFP responses in A1 and AAF, bar represents the duration of the sound.

multiunit extracellular recording to functionally localize these two regions (Fig. 1A, B). Pure tones of different intensity and frequency combinations (0.5–64 kHz, 0.1 octave step; 0–70 dB, 10 dB step) were pseudo-randomly delivered, and the multi-unit responses were obtained using a tungsten electrode (Fig. 1A, see Experimental procedures for details) to reconstruct the tonal receptive field (TRF, Fig. 1C). The CF of every recording site resembled the tonotopic map on the temporal cortex of the animal (Fig. 1B). Identification of A1 and AAF were based on the reversed tonotopic gradient (Doron et al., 2002; Polley et al., 2007; Tao et al., 2017) (Fig. 1B, C). Defining the boundary between A1 and AAF would be arbitrary, given that the high-frequency areas of these two regions are adjacent. However, the 1–10-kHz frequency regions of A1 and AAF are distinctly separate. During the functional identification of A1 and AAF, we transformed the tonotopic map and used the centroid of 1–10-kHz areas as the center to indicate the position of A1 and AAF (Fig. 1D, see Experimental procedures for details). The 1–10-kHz frequency center of AAF was 2.3 ± 0.3 mm (mean ± SD, unless otherwise specified) more anterior ($n = 20$, $p < 0.01$, paired t test), and 1.4 ± 0.3 mm more ventral ($n = 20$, $p < 0.01$, paired t test) than that of A1 (Fig. 1E, F). The goal of this study is to determine whether A1 can modulate the activities of AAF. To avoid any possible artifacts, we specifically modulated the activities of the 1–10-kHz frequency region of A1 and observed the alterations in the responses in the equivalent frequency region in AAF. It should be noted that the positions of A1 and AAF could be variable across different individuals. Therefore, we performed functional mapping before each experiment. To characterize the relative positions of A1 and AAF, we used a vector that started from the center of A1 center and ended at the center of AAF (Fig. 1E). Each vector represents one animal. After aligning the start point (A1) for each animal, we found that the relative positions of A1 and AAF are generally constant across animals (Fig. 1F). AAF is approximately 2 mm anterior and ventral to A1 in each rat. Meanwhile, we characterized the temporal properties for A1 and AAF (Fig. 1G–J). We found no significant difference in the onset latency between A1 (11.4 ± 1.8 ms) and AAF (11.4 ± 2.5 ms, t test, $p = 0.25$) for multi-unit activities (MUA, Fig. 1G–I) and local field potential responses (LFP, Fig. 1J), which is consistent with the previous report in rat (Polley et al., 2007). Comparison of the LFP shape between A1 and AAF can be found in previous report (Reimer et al., 2011).

Activation of A1 axon terminals in AAF

Previous studies have suggested a direct corticocortical projection from A1 to ipsilateral AAF in cats (Carrasco and Lomber, 2009). Here, we wanted to reconfirm this projection with a cell-type-specific approach in rat. We focused on the excitatory projections from A1 to AAF. After functional localization of A1 and AAF, we inject AAV2/8-CaMKIIα-eGFP (see Experimental procedures for details) into A1 of wild-type animals (Fig. 2A, B). This virus can express eGFP under the calcium-calmodulin-dependent kinase II α (CaMKIIα) promoter, which is expressed specifically in excitatory neurons in the cortex thus allowing us anterogradely trace the excitatory projections from A1 to AAF. In AAF, we observed dense axon terminals (Fig. 2B), providing evidence that A1 sends direct excitatory projections to AAF. We also injected cholera toxin subunit B (CTb, see Experimental procedures for details), a retrograde tracer, into AAF (Fig. 2C), and observed labeled cell bodies in all layers of A1 but mostly in layer 2/3 and layer 5 (Fig. 2D).

To investigate whether A1 can modulate neuronal activities in AAF, we injected AAV2/5-CaMKIIα-hChR2-mCherry into A1 to specifically express channelrhodopsin-2 (ChR2) in excitatory neurons. The specificity of the expression of these viruses has been confirmed using immunohistochemistry. We observed the co-localization of CaMKIIa-GFP and ChR2-mCherry in A1 (Fig. 3A, see Experimental procedures for details). The efficiency of ChR2 has been verified for each experiment: light stimulation can reliably evoke spiking responses at the injection site (Fig. 3B). Then we activated neuronal cell bodies in A1 (Fig. 3C) and observed a late (the onset latency of evoked LFPs was about 50 ms) and persistent LFP response in AAF, which is much slower than the LFP response induced by sound stimulation (Fig. 3C).

To test whether A1 can directly modulate responses in AAF through monosynaptic projections, we expressed ChR2 in A1 and obtained

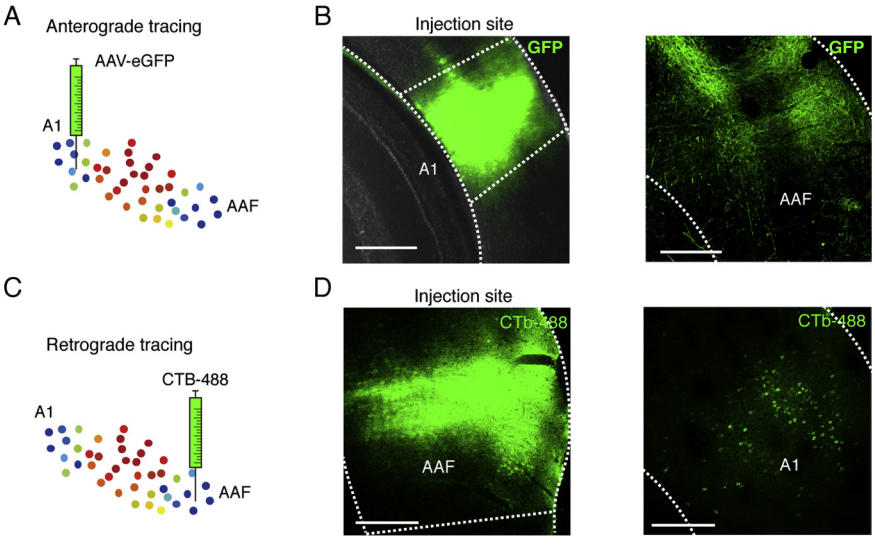

Fig. 2. Excitatory projections from A1 to AAF. (A) Schematic drawing of the anterograde tracing experiments. (B) Left panel, the image shows the expression of eGFP in the injection site (A1); right panel, the image shows the axon terminals in AAF. Bar = 500 μm. (C) Schematic drawing of the retrograde tracing experiments. (D) Left panel, the image shows the injection site; right panel, the image shows labeled cell bodies in A1. Bar = 500 μm.

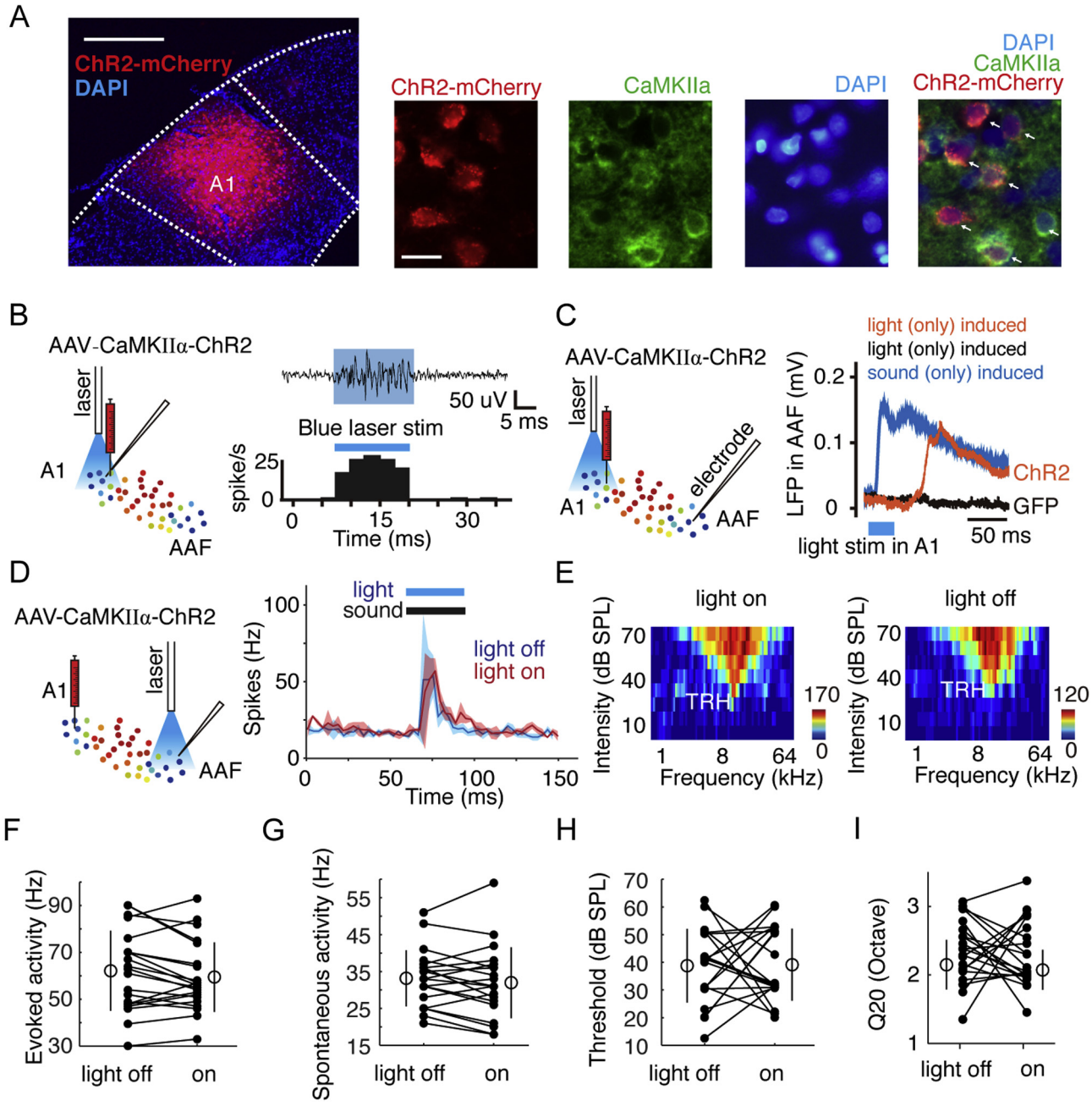

Fig. 3. Activation of A1 axon terminals in AAF. (A) Expression of ChR2 in excitatory neurons in A1. Bar = 600 μm. Right panel, double staining of CaMKIIa and ChR2 in A1; arrows indicate neurons co-expressing CaMKIIa and ChR2. Bar, 30 μm. (B) Photostimulation in A1 and simultaneous recording in A1. Upper right, raw recorded multiunit waveforms; lower right panel, PSTH. (C) Schematic drawing of photostimulation in A1 and simultaneous recording in AAF, right panel, local field potential recorded in AAF when photostimulating A1 in the animal with GFP (black) or ChR2 (orange) expressed in A1, the blue line shows the sound induced LFP in AAF without light stimulation. The shaded area represents standard error. Bar, duration of light or sound stimulation. (D) Left panel, the schematic drawing of photostimulating A1 axon terminals in AAF and simultaneous recording in AAF; right panel, sound-evoked PSTH in AAF under the conditions with and without light stimulation, the shaded area represents standard error. Bars represent the duration of light and sound stimulations. (E) TRFs under light-on and light-off conditions at the same recording site in AAF. TRH, intensity threshold. (F) Sound-evoked activities in AAF in light-off and light-on conditions, $p = 0.12$, paired t test. Error bar, SD, $n = 21$ from three animals. (G) Spontaneous activities in AAF in light-off and light-on conditions, $p = 0.22$, paired t test. Error bar, SD, $n = 21$ from three animals. (H) Intensity threshold in AAF in light-off and light-on conditions, $p = 0.91$, paired t test. Error bar, SD, $n = 21$ from three animals. (I) Q20 in AAF in light-off and light-on conditions, $p = 0.74$, paired t test. Error bar, SD, $n = 21$ from three animals. (For interpretation of the references to color in this figure legend, the reader is referred to the web version of this article.)

sound-evoked responses in AAF while photostimulating A1 axon terminals in AAF (Fig. 3D). We did not observe significant changes of sound-evoked activity in AAF while A1 axon terminals in AAF were activated (Fig. 3D, E). Terminal activation also did not significantly modulate evoked (light off, 62 ± 17 Hz; light on, 59 ± 15 Hz, $p = 0.12$, paired t test, Fig. 3F) and spontaneous activity (light off, 33 ± 8 Hz; light on, 31

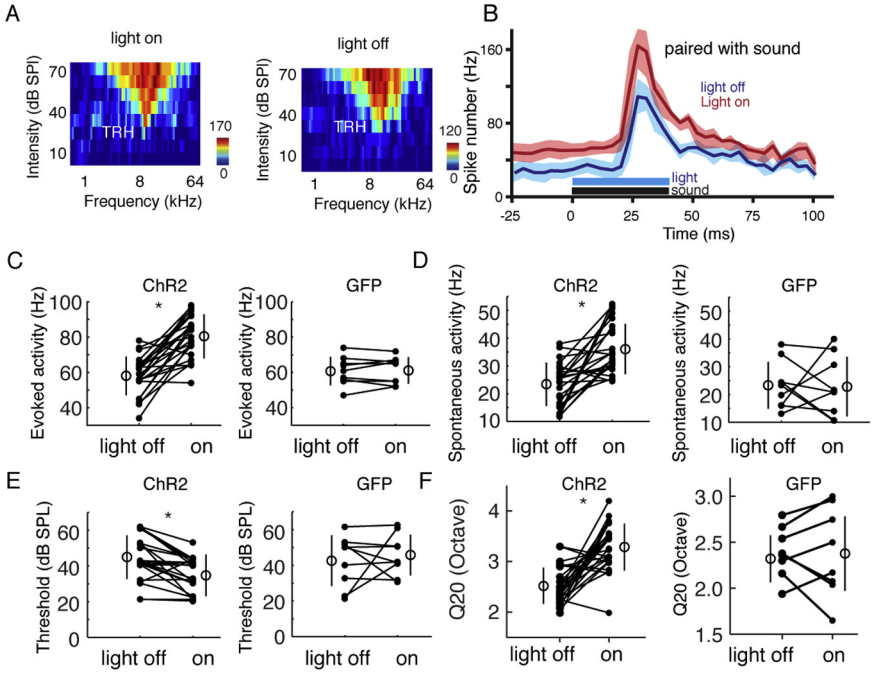

Fig. 4. A1 activation increases the excitability of AAF. (A) Tonal receptive field (TRF) in light-off and light-on conditions at the same recording site in AAF. TRH, intensity threshold. (B) PSTH of light-off and light-on conditions in AAF, shaded area represents standard error. Bars represent the duration of sound and light stimulation. (C) Sound-evoked activities in AAF in light-off and light-on conditions while expressed ChR2 in A1. $^{*}p < 0.001$, paired *t* test. Error bar, SD, $n = 24$ from five animals. Right panel, sound-evoked activities in AAF in light-off and light-on conditions while expressed GFP in A1, $p = 0.77$, paired *t* test, $n = 9$ from two animals. (D) Spontaneous activities in AAF in light-off and light-on conditions while expressed ChR2 in A1. $^{*}p < 0.001$, paired *t* test. Error bar, SD, $n = 24$ from five animals. Right panel, spontaneous activities in AAF on light-off and light-on conditions while expressed GFP in A1, $p = 0.36$, paired *t* test, $n = 9$ from two animals. (E) Intensity threshold in AAF in light-off and light-on conditions while expressed ChR2 in A1. $^{*}p < 0.001$, paired *t* test. Error bar, SD, $n = 24$ from five animals. Right panel, intensity threshold in AAF in light-off and light-on conditions while expressed GFP in A1, $p = 0.58$, paired *t* test, $n = 9$ from two animals. (F) Q20 in AAF in light-off and light-on conditions while expressed ChR2 in A1. $^{*}p < 0.001$, paired *t* test. Error bar, SD, $n = 24$ from five animals. Right panel, Q20 in AAF in light-off and light-on conditions while expressed GFP in A1, $p = 0.84$, paired *t* test, $n = 9$ from two animals.

± 10 Hz, $p = 0.22$, paired *t* test, Fig. 3G), and intensity threshold (light off, 38 ± 13 dB; light on, 38 ± 13 dB, $p = 0.91$, paired *t* test, Fig. 3H) and the bandwidth at 20 dB above threshold (Q20, light off, 2.2 ± 0.3 octave; light on, 2.1 ± 0.2 octave, $p = 0.74$, paired *t* test, Fig. 3I). These results suggest that A1 cannot modulate responses in AAF through direct ipsilateral corticocortical projections.

Activating A1 neurons increases the excitability of AAF neurons

However, above results did not exclude the possibility that A1 can modulate responses in A1 through indirect connections. Then we investigated whether A1 activation would influence the auditory-evoked responses in AAF. We paired light stimulation (in A1) with an auditory stimulus (60 dB white noise or tones) and compared the responses with and without light stimulation (Fig. 4A, B). We found that the sound-evoked spike number in AAF while A1 was activated (75 ± 10 Hz) was higher than in the control group (62 ± 8, $p < 0.001$, paired *t* test, Fig. 4C), which has not been observed in animals that expressed enhanced green fluorescent protein (eGFP, $p = 0.77$, paired *t* test, Fig. 4C) in A1. In addition, the spontaneous activity increased (from 28 ± 7 Hz to 37 ± 8 Hz, $p < 0.001$, paired *t* test) while A1 was activated (Fig. 4D), which was not observed in animals that express GFP in A1 ($p = 0.36$, paired *t* test, Fig. 4D). After reconstructing the TRF (Fig. 4A), we found that the intensity threshold of AAF while A1 had been activated was decreased (from 44 ± 6 dB to 38 ± 4 dB, $p = 0.008$, paired *t* test) compared to the control group (Fig. 4E). We also compared Q20 before and after light stimulation, and we found that the bandwidth increased (from 2.5 ± 0.4 octave to 3.3 ± 0.5 octave, $p < 0.001$, paired *t* test) in the group in which A1 had been activated (Fig. 4F), but not in the control group ($p = 0.838$, paired *t* test). Considering that A1 terminal activation in AAF did not elicit monosynaptic transient responses in AAF (Fig. 3C), these results suggested that A1 modulate the excitability of AAF through an indirect pathway, for example, the cortico-thalamic connections.

Suppressing A1 decreases responses in AAF

In the above results, we have found that A1 activation facilitated the responses in AAF. Next, we applied an optogenetic approach to evaluating whether A1 deactivation can produce the opposite effects. We injected AAV2/8-CaMKIIa-eNpHR3.0-eYFP virus into A1 to specifically express eNpHR3.0 on the membrane of the excitatory neurons (Fig. 5A). These light-activated channels permit Cl(−) into the neurons while activated, thereby hyperpolarizing the membrane potential, which in turn suppresses neuronal activity (Gradinaru et al., 2008). We verified the specificity of the expression of NpHR3.0 using immunohistochemistry (Fig. 5A). The efficiency of A1 suppression was verified before each experiment: we recorded multiunit activities in A1 while simultaneously delivering light stimulation on the surface of A1 (Fig. 5B, C). We confirmed that the light stimulation could suppress (from 64 ± 9 to 48 ± 7, paired *t* test, $p = 0.031$) the sound-evoked responses in A1 (Fig. 5D).

To investigate how A1 suppression would affect the information processing in AAF, we recorded the sound-evoked responses in AAF while delivering light stimulation to activate the eNpHR3.0 channels in A1 (Figs. 5E, 3F, H). By comparing TRF between light-on

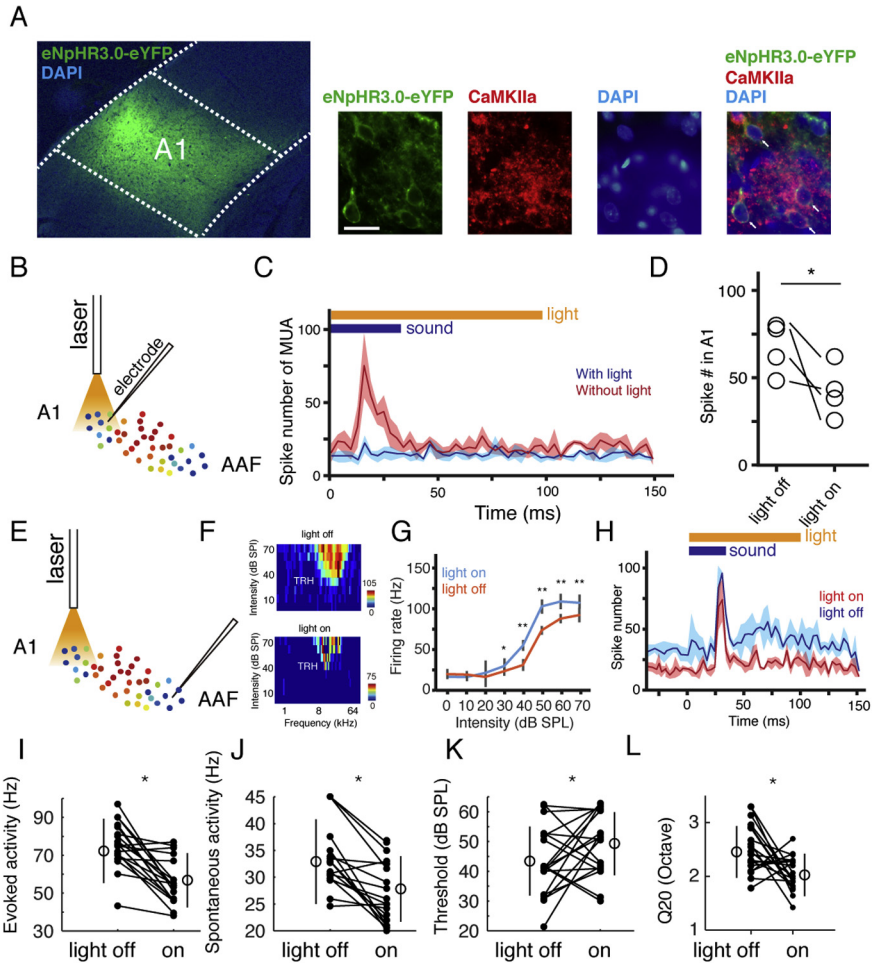

Fig. 5. Suppressing A1 decreased the excitability of AAF. (A) Expression of eNpHR3.0 in A1. Right panel, double staining of CaMKIIa and ChR2 in A1; arrows indicate neurons co-expressed eNpHR3.0 and CaMKIIa. Bar = 30 μm. (B) Schematic of photostimulation in A1 and simultaneous recording in A1. (C) Sound-evoked PSTH in A1 under the conditions with and without light stimulation, the shaded area represents standard error. Bar, duration of light and sound stimulation. (D) Statistics represent the effective suppression of A1 activity. $^{*}p = 0.031$, paired t test, $n = 4$. (E) Schematic drawing of recording responses in AAF during photostimulation of A1. (F) TRF in light-off and light-on conditions at the same recording site in AAF. TRH, intensity threshold. (G) Spiking rate versus intensity under light-on and light-off conditions. Error bar, SEM, $n = 8$ from two animals, $^{*}p < 0.05$, $^{**}p < 0.01$, student t test. (H) PSTH of light-off and light-on conditions in AAF, shaded area represents standard error. Bars represent the duration of sound and light stimulation. (I) Sound-evoked activities in AAF in light-off and light-on conditions while expressed eNpHR3.0 in A1, $p = 0.02$, paired t test. Error bar, SD, $n = 19$ from four animals. (J) Spontaneous activities in AAF in light-off and light-on conditions while expressed eNpHR3.0 in A1, $p = 0.02$, paired t test. Error bar, SD, $n = 19$ from four animals. (K) Intensity threshold in AAF in light-off and light-on conditions while expressed eNpHR3.0 in A1, $p = 0.03$, paired t test. Error bar, SD, $n = 19$ from four animals. (L) Q20 in AAF in light-off and light-on conditions while expressed eNpHR3.0 in A1, $p = 0.006$, paired t test. Error bar, SD, $n = 19$ from four animals.

and light-off conditions, we found the monotonicity pattern did not change, but the response strength decreased while A1 was deactivated (Fig. 5G). Compared with the control group (without light stimulation), light stimulation decreased both the evoked (from 73 ± 8 Hz to 53 ± 9 Hz, $p = 0.02$, paired t test, Fig. 5I) and the spontaneous responses (from 32 ± 5 Hz to 27 ± 4 Hz, $p = 0.02$, paired t test, Fig. 5J) in AAF. In addition, when we compared the TRF, we found that the intensity threshold increased (from 43 ± 4 dB to 48 ± 5 dB, $p = 0.03$, paired t test, Fig. 5K) while A1 was suppressed, and the bandwidth (Q20) decreased (2.5 ± 0.4 octave to 2.1 ± 0.3 octave, $p = 0.006$, paired t test, Fig. 5L). These results show that the A1 suppression decreased the general excitability of AAF.

DISCUSSION

To investigate the influence of A1 on the sound-evoked responses in ipsilateral AAF, we used cell-type-specific anterograde tracing and observed direct excitatory projections from A1 to ipsilateral AAF. We used an optogenetic approach to manipulate the activity of A1 and recorded the sound-evoked responses in ipsilateral AAF, but A1 axon terminal activation in AAF did not alter the tone-evoked responses in AAF. However, we found that activation of excitatory cell bodies in A1 increased the spontaneous and sound-evoked responses in AAF and that suppression of A1 decreased the responses in AAF. Our results suggest that A1 could modulate the general excitability in AAF through an indirect pathway.

Parallel auditory ascending pathways

In the visual cortex, silencing the primary visual cortex (V1) results in suppression of the secondary visual cortex (V2); thus, it has been proposed that visual information is serially processed: visual information is transferred from V1 to V2 (Girard and Bullier, 1989; Girard et al., 1991). However, in the somatosensory cortex (Pons et al., 1987; Turman et al., 1995), both serial and parallel processing pathways have been proposed, and the overall processing remains ambiguous. Thus, different modalities might adopt different strategies for information processing. In the auditory cortex, it has been speculated that A1 and AAF are parallel auditory ascending pathways, and our results are consistent with this deduction. In rat, A1 and AAF (Fig. 1B) are tonotopically organized regions, and both can receive direct ascending auditory input from thalamus (Ehret and Romand, 1997; Polley et al., 2007). In our study, no significant difference has been found in the onset latencies of sound-evoked responses between A1 and AAF (Fig. 1G–J), which is consistent with previous

reports in rats (Polley et al., 2007; Reimer et al., 2011). Optogenetic deactivation of A1 did not result in silencing of AAF; instead, it simply decreased the firing rate of AAF (Fig. 5); optogenetic activation of A1 did not evoke transient responses in AAF (Fig. 4A), which suggested that the auditory responses in AAF were not inherited from A1.

A1 modulates the excitability of AAF

Classic approaches have previously been used to investigate the interactions between different regions in the auditory cortex. One study that used reversible cooling to suppress A1 did not find a significant alteration in AAF activities in cats (Carrasco and Lomber, 2009). However, limited by this technique, cell-type specificity cannot be verified, and the modulation of cortical activity can only be unidirectional (deactivation). With the optogenetic approach, we can specifically and reversibly activate/deactivate A1. In this study, A1 activation increased the spontaneous and evoked responses in AAF, decreased the sound intensity threshold of the TRF, and broadened the bandwidth (Fig. 4), while A1 deactivation caused the opposite effects (Fig. 5). Our anatomical results (Fig. 2) were consistent with previous reports that A1 sends abundant projections to AAF (Ehret and Romand, 1997; Kaas and Hackett, 2000; Bizley and Cohen, 2013). Direct activation of excitatory neurons in A1 did not evoke transient spiking responses in AAF, but a persistent and late (latency >50 ms) response (Fig. 4A), and A1 axon terminal activation did not change the response property of AAF (Fig. 3). These results suggested that the excitatory effect did not depend on the direct projections from A1 to ipsilateral AAF. Previous studies reported that bilateral auditory cortices, as well as the subcortical nuclei and the auditory cortex (e.g. medial geniculate body), were reciprocally connected in cats (Andersen et al., 1980; Games and Winer, 1988; Herbert et al., 1991; Winer et al., 2001). Meanwhile, A1 can project to the part of the thalamus that project to AAF in the cat (Andersen et al., 1980). Deactivation of A1 would modulate the response properties of contralateral AAF (Carrasco et al., 2015). The excitation-inhibition balance could determine the cortical activity (Wehr and Zador, 2003; Higley and Contreras, 2006; Tao et al., 2016), so it is possible that A1 is capable to modulate the E–I balance in AAF via either bilateral corticocortical connections or the thalamocortical circuits. However, further investigations are needed to directly test these possibilities. Based on the latency of onset responses in A1 and AAF, any sound-evoked responses would reach A1 and AAF simultaneously. Thus, the relatively slow modulation effect of A1 on AAF can only affect the subsequent responses in AAF, suggesting that this kind of modulation might be involved in the processing of long-duration sound, waveform envelope profiles or cortical plasticity. In conclusion, our results reveal a salient excitatory effect of A1 on AAF using an optogenetic approach that specifically activates or suppress the activity of A1 excitatory neurons.

DISCLOSURE/CONFLICT-OF-INTEREST STATEMENT

The authors declare no competing financial interests.

AUTHOR CONTRIBUTIONS

C.T., G.Z., Y.Z. and Y.X. discussed and wrote the manuscript. C.T. and G.Z. performed the virus injection, obtained the electrophysiological data and prepared the figures. C.T. collected the imaging data. C.Z., L.W. S.Y. and Z.W. performed the immunohistochemistry experiments. Y.Z. and Y.X. designed the experiments and supervised the work.

Acknowledgments—This work was supported by grants from National Natural Science Foundation of China (31471056, 31371116 and 31271177) and the State Key Laboratory of Neuroscience (No. SKLN-2015B01).

REFERENCES

Andersen RA, Knight PL, Merzenich MM (1980) The thalamocortical and corticothalamic connections of AI, AII, and the anterior auditory field (AAF) in the cat: evidence for two largely segregated systems of connections. J Comp Neurol 194:663–701.

Bizley JK, Cohen YE (2013) The what, where and how of auditory-object perception. Nat Rev Neurosci 14:693–707.

Carrasco A, Lomber SG (2009) Differential modulatory influences between primary auditory cortex and the anterior auditory field. J Neurosci 29:8350–8362.

Carrasco A, Kok MA, Lomber SG (2015) Effects of core auditory cortex deactivation on neuronal response to simple and complex acoustic signals in the contralateral anterior auditory field. Cereb Cortex 25:84–96.

Doron NN, Ledoux JE, Semple MN (2002) Redefining the tonotopic core of rat auditory cortex: physiological evidence for a posterior field. J Comp Neurol 453:345–360.

Ehret G, Romand R (1997) The central auditory system. New York: Oxford University Press.

Games KD, Winer JA (1988) Layer V in rat auditory cortex: projections to the inferior colliculus and contralateral cortex. Hear Res 34:1–25.

Girard P, Bullier J (1989) Visual activity in area V2 during reversible inactivation of area 17 in the macaque monkey. J Neurophysiol 62:1287–1302.

Girard P, Salin PA, Bullier J (1991) Visual activity in areas V3a and V3 during reversible inactivation of area V1 in the macaque monkey. J Neurophysiol 66:1493–1503.

Gradinaru V, Thompson KR, Deisseroth K (2008) ENpHR: a natronomonas halorhodopsin enhanced for optogenetic applications. Brain Cell Biol 36:129–139.

Guo W, Chambers AR, Darrow KN, Hancock KE, Shinn-Cunningham BG, Polley DB (2012) Robustness of cortical topography across fields, laminae, anesthetic states, and neurophysiological signal types. J Neurosci 32:9159–9172.

Hackett TA, Barkat TR, O'brien BM, Hensch TK, Polley DB (2011) Linking topography to tonotopy in the mouse auditory thalamocortical circuit. J Neurosci 31:2983–2995.

Herbert H, Aschoff A, Ostwald J (1991) Topography of projections from the auditory cortex to the inferior colliculus in the rat. J Comp Neurol 304:103–122.

Higley MJ, Contreras D (2006) Balanced excitation and inhibition determine spike timing during frequency adaptation. J Neurosci 26:448–457.

Imaizumi K, Priebe NJ, Crum PA, Bedenbaugh PH, Cheung SW, Schreiner CE (2004) Modular functional organization of cat anterior auditory field. J Neurophysiol 92:444–457.
Issa JB, Haeffele BD, Agarwal A, Bergles DE, Young ED, Yue DT (2014) Multiscale optical Ca2+ imaging of tonal organization in mouse auditory cortex. Neuron 83:944–959.
Joachimsthaler B, Uhlmann M, Miller F, Ehret G, Kurt S (2014) Quantitative analysis of neuronal response properties in primary and higher-order auditory cortical fields of awake house mice (Mus musculus). Eur J Neurosci 39:904–918.
Kaas JH, Hackett TA (2000) Subdivisions of auditory cortex and processing streams in primates. Proc Natl Acad Sci U S A 97:11793–11799.
Lee CC, Winer JA (2008) Connections of cat auditory cortex: II. Commissural system. J Comp Neurol 507:1901–1919.
Lee CC, Schreiner CE, Imaizumi K, Winer JA (2004) Tonotopic and heterotopic projection systems in physiologically defined auditory cortex. Neuroscience 128:871–887.
Morel A, Imig TJ (1987) Thalamic projections to fields A, AI, P, and VP in the cat auditory cortex. J Comp Neurol 265:119–144.
Polley DB, Read HL, Storace DA, Merzenich MM (2007) Multiparametric auditory receptive field organization across five cortical fields in the albino rat. J Neurophysiol 97:3621–3638.
Pons TP, Garraghty PE, Friedman DP, Mishkin M (1987) Physiological evidence for serial processing in somatosensory cortex. Science 237:417–420.
Reimer A, Hubka P, Engel AK, Kral A (2011) Fast propagating waves within the rodent auditory cortex. Cereb Cortex 21:166–177.
Rouiller EM, Simm GM, Villa AE, De Ribaupierre Y, De Ribaupierre F (1991) Auditory corticocortical interconnections in the cat: evidence for parallel and hierarchical arrangement of the auditory cortical areas. Exp Brain Res 86:483–505.
Rutkowski RG, Miasnikov AA, Weinberger NM (2003) Characterisation of multiple physiological fields within the anatomical core of rat auditory cortex. Hear Res 181:116–130.
Shiramatsu TI, Noda T, Akutsu K, Takahashi H (2016) Tonotopic and field-specific representation of long-lasting sustained activity in rat auditory cortex. Front Neural Circuits 10:59.
Tao C, Zhang G, Zhou C, Wang L, Yan S, Zhang LI, Zhou Y, Xiong Y (2016) Synaptic Basis for the Generation of Response Variation in Auditory Cortex. Sci Rep 6:31024.
Tao C, Zhang G, Zhou C, Wang L, Yan S, Tao HW, Zhang LI, Zhou Y, Xiong Y (2017) Diversity in excitation-inhibition mismatch underlies local functional heterogeneity in the rat auditory cortex. Cell Rep 19:521–531.
Turman AB, Morley JW, Zhang HQ, Rowe MJ (1995) Parallel processing of tactile information in cat cerebral cortex: effect of reversible inactivation of SII on SI responses. J Neurophysiol 73:1063–1075.
Wehr M, Zador AM (2003) Balanced inhibition underlies tuning and sharpens spike timing in auditory cortex. Nature 426:442–446.
Winer JA, Sally SL, Larue DT, Kelly JB (1999) Origins of medial geniculate body projections to physiologically defined zones of rat primary auditory cortex. Hear Res 130:42–61.
Winer JA, Diehl JJ, Larue DT (2001) Projections of auditory cortex to the medial geniculate body of the cat. J Comp Neurol 430:27–55.

(Received 11 February 2017, Accepted 9 August 2017)
(Available online 19 August 2017)